Journal of the Mechanical Behavior of Biomedical Materials 82 (2018) 383–393

Contents lists available at ScienceDirect

Journal of the Mechanical Behavior of Biomedical Materials

journal homepage: www.elsevier.com/locate/jmbbm

Droplet based vitrification for cell aggregates: Numerical analysis

Meng Shi[a,b], Shangsheng Feng[b,c], Xiaohui Zhang[b,d], Changchun Ji[b,d], Feng Xu[b,d,*], Tian Jian Lu[b,c,e,**]

[a] School of Energy and Power Engineering, Xi'an Jiaotong University, Xi'an 710049, PR China
[b] Bioinspired Engineering and Biomechanics Center (BEBC), Xi'an Jiaotong University, Xi'an 710049, PR China
[c] State Key Laboratory of Mechanical Structure Strength and Vibration, School of Aerospace, Xi'an Jiaotong University, Xi'an 710049, PR China
[d] MOE Key Laboratory of Biomedical Information Engineering, School of Life Science and Technology, Xi'an Jiaotong University, Xi'an 710049, PR China
[e] MOE Key Laboratory of Multifunctional Structures and Materials, Xi'an Jiaotong University, Xi'an 710049, PR China

ARTICLE INFO

Keywords:
Cell aggregates
Vitrification
Simulation
Cell membrane

ABSTRACT

Cell aggregates represent the main format of cells existing *in vivo* and have been widely used as tissue and disease models *in vitro*. Nevertheless, the preservation of cell aggregates while maintaining their functionalities for off-the-shelf applications is still challenging. Among various preservation methods, droplet-based vitrification exhibits superior advantages for the cryopreservation of cell aggregates; however, the physical mechanisms underlying droplet-based vitrification of cell aggregate using this method remain elusive. To address this issue, we proposed a voronoi model to construct two-dimensional geometric morphologies of cell aggregates and established a coupled physical model to describe the diffusion, heat transfer and crystallization processes during vitrification. Based on these models, we performed a numerical study on the variation and distribution of cryoprotectant (CPA) concentration, temperature and crystallization in cell aggregates during droplet-based vitrification. The results show that although cell membrane is not an obvious barrier in heat transfer, it affects the diffusion of CPA remarkably as a biologic film and thus the following crystallization in cell aggregates. The effective protection of CPA during vitrification occurs during the initial stage of CPA diffusion, thus a longer CPA loading time does not necessarily lead to significant decrease in crystallization, but rather may induce more toxicity to cells.

1. Introduction

Plentiful cells in the living system exist in the form of aggregates *in vivo*, such as islets, embryos, cancer tumor, and alveoli (Ewald, 2017; Ma et al., 2017; Rawal et al., 2017; Yamamoto et al., 2017). Significant efforts have been devoted to developing cell aggregates such as embryonic bodies (EBs) and tumor aggregates as they can closely mimic the native situation compared to monolayer cells, thus more ideal for constructing tissue or disease models *in vitro* (Asghar et al., 2015; Chan et al., 2013; Souza et al., 2010; Takagi et al., 2016). For instance, tumor aggregates have been frequently used in the research of tumor biology, drug screening, *etc.* (Fan et al., 2016; Friedrich et al., 2009). EBs are a typical model system to recapitulate certain features of native embryonic development, *e.g.*, differentiation of embryo into three germ layers (Wei et al., 2016; Xu et al., 2011). More recently, cell spheroids have been employed as an important component of the organ-on-a-chip platform, which emerges as a powerful tool in biomedical applications, such as pathology studies and drug screening (Skardal et al., 2017; Yang et al., 2017). For off-the-shelf applications, cell spheroids require to be preserved with maintained viability and functionalities, which however is challenging due to the large size of cell aggregates (*e.g.*, hundreds of microns in size).

Cryopreservation has been widely used to preserve cells, cell aggregates, tissues and other organisms, showing great promise of organ and tissue preservation (Giwa et al., 2017). Although conventional and programmable cryopreservation has successfully preserved suspended cells (da Fonseca Cardoso et al., 2017; Li et al., 2010), existing methods are associated with certain limitations for cryopreservation of relatively large cell aggregates, resulting in low cooling rate, high ice formation during cooling and thus the destruction of survival rate and structure of cell aggregates. In comparison, vitrification, as an ultra-fast cooling and ice-free method, holds great potential in preserving large biospecimens (Khosla et al., 2017; Manuchehrabadi et al., 2017), with advantages in better maintaining cell viability, genetic profiles and cytoskeletal structure (Dou et al., 2015; Kuleshova et al., 2007; Magalhães et al., 2012; Shi et al., 2015). As a representative, inspired by recent advances

* Corresponding author at: Bioinspired Engineering and Biomechanics Center (BEBC), Xi'an Jiaotong University, Xi'an 710049, PR China.
** Corresponding author at: MOE Key Laboratory of Multifunctional Structures and Materials, Xi'an Jiaotong University, Xi'an 710049, PR China
E-mail addresses: fengxu@mail.xjtu.edu.cn (F. Xu), tjlu@mail.xjtu.edu.cn (T.J. Lu).

https://doi.org/10.1016/j.jmbbm.2018.03.026
Received 28 November 2017; Received in revised form 6 February 2018; Accepted 21 March 2018
Available online 22 March 2018
1751-6161/

in bioprinting technology (Gao et al., 2016; Xu et al., 2011; Zhang et al., 2012b), the droplet-based vitrification method, which generates droplets encapsulating cells and injects them into liquid nitrogen directly, has emerged as a convenient and efficient way to freeze cells (El Assal et al., 2014).

During droplet-based vitrification, when the temperature decreases to the solidifying point, the liquid starts to be solidified. There are three critical temperature points, *i.e.*, the melting temperature, the nucleation temperature and the glass transition temperature (vitrification temperature), denoted here as T_m, T_h and T_g, respectively. Intracellular ice formation in the temperature region between T_m and T_g, *i.e.*, the so-called Dangerous Temperature Region (DTR) (Song et al., 2010), is the main killer for the cells during cooling. As the cooling rate of droplet-based vitrification is sufficiently high, *e.g.*, up to 10^6 °C/min (Isachenko et al., 2004), it can go through the DTR quickly to minimize crystal formation. The droplet after cooling can be regarded as a glass droplet (amorphous ice). Thus, the cells and cells' inner structure can be preserved from damage induced by ice formation to maintain high survival rates.

Due to its high efficiency, droplet-based vitrification has been widely utilized in the cryopreservation of cells, such as fibroblast cells (Dou et al., 2015), hepatocytes cells (Demirci and Montesano, 2007), red blood cells (El Assal et al., 2014) and oocytes (Zhang et al., 2012b). However, at present, only very few successful droplet-based vitrification of cell aggregates (*e.g.,* mouse embryos) were reported (An et al., 2015; Dhali et al., 2009). This is mostly due to limited understandings of the physical processes (*e.g.*, crystallization, heat and mass transfer) and critical factors (*e.g.*, aggregates size, cooling time and cell membrane effect) in droplet vitrification of cell aggregates, causing difficulty in designing optimal vitrification approaches. For instance, it is still not clear whether cell membrane plays a critical role during droplet vitrification of cell aggregates. Although a few models have provided helpful predictions of droplet based vitrification of single cell (Ryoun Youn and Seok Song, 2012; Xu et al., 2010), there is still a high demand of numerical models for droplet based vitrification of cell aggregates to understand the physics in these more complex structures.

In the current study, we performed a numerical investigation on vitrification of cell aggregates encapsulated in microdroplets. We coupled the equations of diffusion, crystallization and heat transfer to describe the physical processes of vitrification cryopreservation. Specifically, we developed a geometry model based on voronoi polygons to mimic the morphology of cell aggregates. The cell membrane was accounted for by the model to evaluate its effects on diffusion, heat transfer and crystallization during vitrification. We also quantified the effects of CPA loading time and cell aggregate diameter on cryopreservation. This work provides a guidance in the experimental design of droplet-based vitrification for cell aggregates having relatively large size.

2. Methods

2.1. Numerical method

2.1.1. Geometry model of cell aggregates

Cell aggregates in living organisms consist of a number of cells side by side, which typically stay tight to each other in spheroidal morphology that presents the appearance of polygons, such as epithelium cell aggregates, ectoderm aggregates, progenitor cell aggregates, tumors and embryos (Fierro-González et al., 2013; Krieg et al., 2008; Lecuit and Lenne, 2007; Florczyk et al., 2012; Manning et al., 2010). This geometrical order optimizes the packing of cells and minimizes the surface energy in whole cell aggregates (Lecuit and Lenne, 2007; Pedersen et al., 1999). Inspired by the top view of cancer cells aggregates (Florczyk et al., 2012) (Fig. 1**a**), the morphology of "voronoi" polygons is used to mimic the geometry of cell aggregates (Fig. 1). This geometry model rebuilds cell shapes based on cellular physical interaction forces, which may be regarded as a representative cross-section of cell aggregate to illustrate its inner variation during vitrification.

The geometry model of cell aggregates is drawn using MATLAB™, with redundant lines modified using AUTOCAD™ before importing into the computational software (Fig. 1**b-d**). In this geometry model, the diameter of cell aggregate, cell size and quantity can be designed conveniently. To better mimic droplet-based vitrification, we utilized a concentric annulus to represent CPA solution surrounding the cell aggregate during vitrification. We selected a fixed droplet diameter of 200 μm, which is within the size range of droplets generated by most systems such as microfluidics and cell printing system (Xu et al., 2011). Given the size range of most native cell aggregates like islets and cancer acini (Zhang et al., 2012a), cell aggregate encapsulated in droplets have a diameter of 50 μm, 100 μm, and 150 μm, containing a total of 15, 56, and 103 cells, respectively. Since we considered the polygon shape of cell aggregates as shown in Fig. 1**a**, in the proposed geometry model the cells stay close to each other without space except for cell membrane.

To evaluate the influence of cell membrane on vitrification, we defined a 10 nm distance between adjacent cells to represent the cell membrane (Korn, 1966) (Fig. 1**e**). Due to lack of experimental data on the thermal properties of cell membranes, we referred to the thermal conductivity of human tissues (Bowman et al., 1975; Choi and Bischof, 2010) and initially chose $\lambda_0 = 0.4$ W/(m·K) as cell membrane conductivity for our simulation (Table 1). Subsequently, to guarantee the accuracy of numerical simulation, we also varied the membrane conductivity as 0.04, 0.4, 4, and 40 (W/(m·K), which covered most biologic tissues (Bowman et al., 1975; Choi and Bischof, 2010; Hamilton, 1998). Further, we assumed that each polygonal cell has homogeneous properties within the cell membrane. Thus, in the proposed model, there existed three regions with different properties, *i.e.*, the CPA layer, the inner cell domain, and the cell membrane.

2.1.2. Governing equations

2.1.2.1. Before cooling. CPA loading is an essential step in vitrification cryopreservation: a cell aggregate is exposed to a certain concentration of CPA, which then diffuses through cell membrane into cells to partly replace water within the cells. Thus, mass transfer of CPA occurs across the boundary to eventually reach the center of the aggregate and change the characteristic parameters of cells to avoid crystallization in vitrification. For relatively large tissues such as cell aggregates, the diffusion equation for conservation of chemical species was used to predict the mass transfer of CPA, as (Lawson et al., 2012; Lee and Rubinsky, 1989):

$$\frac{\partial c}{\partial t} = D\nabla^2 c \tag{1}$$

where c (mol/m^3) is the concentration of CPA, t (s) is the time, and D (m^2/s) is the diffusivity of CPA, with a magnitude of 1×10^{-9} m^2/s for cell (Stewart, 1998) and 1.0×10^{-13} m^2/s for cell membrane (Lieb and Stein, 1972). In the calculation, CPA concentration at the boundary of cell aggregate was assumed to be equal to that of the surrounding CPA solution ($c_0 = 4200$ mol/m^3) since cell aggregate is exposed to CPA solution during CPA loading process. Three important values of CPA concentration were chosen to investigate the variation of CPA in cell aggregate, namely, when the integral average of CPA concentration (c_i) equals the initial concentration (0), half of surrounding CPA solution concentration ($c_{.5}$), and surrounding CPA solution concentration (c_0). As a representative, the 1,2-propanediol was selected as the CPA solution in this study, which is commonly used in vitrification cryopreservation (Zhang et al., 2004).

As a result of CPA diffusion, the concentration of CPA varies across the cell aggregate and hence the thermal properties of cell aggregate are altered. Let c_i represent the average CPA concentration in cell aggregate after diffusion process is complete. Relevant thermal properties of cell aggregates considered in this study include λ_i, ρ_i, $c_{p,i}$, α_i, $T_{m,i}$ and L_i,

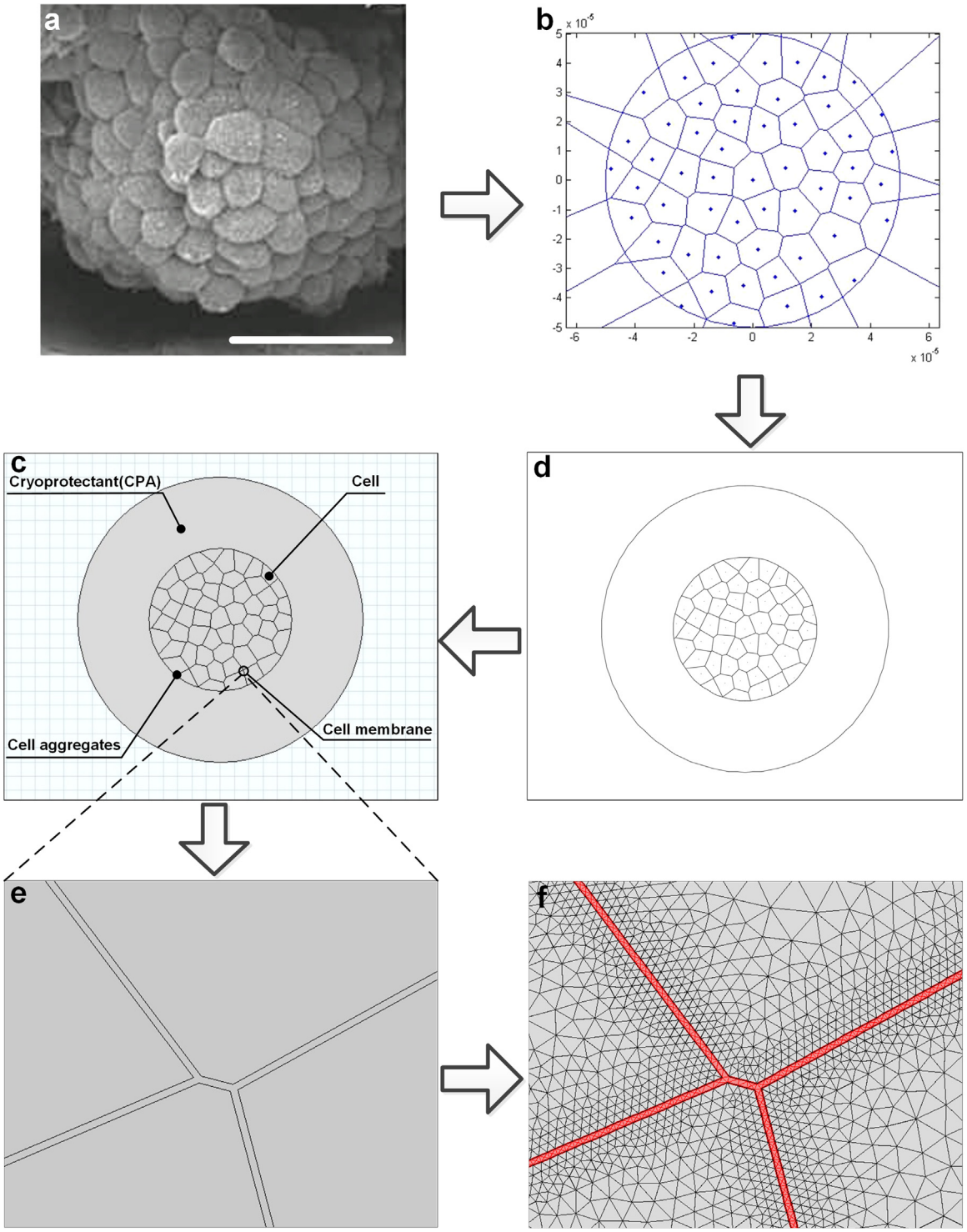

Fig. 1. Two-dimensional geometric model of cell aggregate created based on Voronoi polygon. (a) Cell pattern in aggregate, scale bar: 40 μm (Florczyk et al., 2012), reprinting permission has been authorised by publisher; (b) MATLAB™ image of cell aggregate created by voronoi method; (c) Geometric model of cell aggregate modified by AUTOCAD™; (d) Geometric model of cell aggregate in COMSOL™; (e) Enlarged view of cell membrane; (f) Meshes of cells and cell membrane (red part was cell membrane and cells were located on both sides of cell membrane).

which are quantified by the equations given below.

Thermal conductivity:

$$\lambda_i = (\lambda_{CPA} - \lambda_{cell})\frac{c_i}{c_0} + \lambda_{cell} \quad (2)$$

Density:

$$\rho_i = (\rho_{CPA} - \rho_{cell})\frac{c_i}{c_0} + \rho_{cell} \quad (3)$$

Specific heat capacity:

$$c_{p,i} = (c_{p,CPA} - c_{p,cell})\frac{c_i}{c_0} + c_{p,cell} \quad (4)$$

Thus, the thermal diffusivity is:

Table 1
Thermal conductivity of selected human tissues (Bowman et al., 1975; Choi and Bischof, 2010).

Tissue	Thermal conductivity [W/(m·K)]
Skin	0.476
Cheek	0.487
Brain	0.503
Muscle	0.385
Leg	0.450

$$\alpha_i = \frac{\lambda_i}{\rho_i c_{p,i}} = \frac{(\lambda_{CPA} - \lambda_{cell})\frac{c_i}{c_0} + \lambda_{cell}}{((\rho_{CPA} - \rho_{cell})\frac{c_i}{c_0} + \rho_{cell})((c_{p,CPA} - c_{p,cell})\frac{c_i}{c_0} + c_{p,cell})} \quad (5)$$

Melting temperature:

$$T_{m,i} = (T_{m,CPA} - T_{m,cell})\frac{c_i}{c_0} + T_{m,cell} \quad (6)$$

Latent heat:

$$L_i = (L_{CPA} - L_{cell})\frac{c_i}{c_0} + L_{cell} \quad (7)$$

As water is the major component of most biological tissues, the thermal properties of cells are close to those of water (Hamilton, 1998; Park et al., 2013; Sansinena et al., 2011). Consequently, in the present study, the thermal properties of cells were taken as those of water in COMSOL™ Material Library to consider the effect of temperature on thermal properties during cooling. The thermal properties of CPA (*i.e.*, 1,2-propanediol) can be found in previous literatures (Choi and Bischof, 2010; Flick, 1998; Jabrane et al., 1995; Martin et al., 1999; Zhang et al., 2004). As CPA diffusion process occurs before vitrification cooling, it was computed first. Once CPA diffusion was determined, the updated thermal properties by Eqs. (2)–(7) were employed to simulate subsequent cooling and crystallization processes. As the time scale of vitrification (~seconds) is usually much rapider than CPA diffusion (~minutes) (Zhang et al., 2011, 2012b), CPA diffusion during cooling was ignored.

2.1.2.2. During cooling. Cell aggregates with different diameters are encapsulated in CPA droplets, which are then ejected into liquid nitrogen (77 K). The droplet will first float on the surface of liquid nitrogen due to Leidenfrost effect, then cooled by liquid nitrogen and its surrounding vapor. In the liquid nitrogen container, a vapor layer always exists all over the surface of liquid nitrogen due to its evaporation, and the vapor becomes colder as the liquid nitrogen is approached (Seo and Jeong, 2010). Thus, for a sufficiently small droplet (*e.g.,* diameter 200 μm in this work), although the droplet will levitate on the surface of liquid nitrogen, its location is close to the surface where cold vapor exists. Thus, not only the bottom surface of the droplet is surrounded by nitrogen vapor due to the Leidenfrost phenomenon, but also its top is wreathed by cold nitrogen vapor. After cooling, the droplet will be immersed in the liquid nitrogen, indicating the vitrification process is complete (Song et al., 2010). Based on this mechanism, the vitrification can be divided into two physical processes, *i.e.*, the heat transfer process and the crystallization process, which are coupled with each other. Equations governing crystallization and heat transfer processes are presented below.

2.1.2.3. Crystallization. The non-isothermal kinetic equation (Boutron and Mehl, 1990) was employed to describe the crystallization process, as:

$$\frac{d\chi}{dt} = k_a \chi^{\frac{2}{3}}(1-\chi)(T_m - T)e^{-Q/RT} \quad (8)$$

where χ (-) represents the degree of crystallization ($0 < \chi < 1$). t (s) is the time, and T (K) is the temperature of droplet. T_m (K) is the temperature at the end of melting, Q (J/mol) is the activation energy, and R (J/mol·K) is the gas constant. k_a is the characteristic coefficient of crystallization (Boutron, 1986). Upon coupling with the diffusion process of Eq. (6), Eq. (8) could be rewritten as:

$$\frac{d\chi}{dt} = k_a \chi^{\frac{2}{3}}(1-\chi)((T_{m,CPA} - T_{m,cell})\frac{c_i}{c_0} + T_{m,cell} - T)e^{-Q/RT} \quad (9)$$

2.1.2.4. Heat transfer. The time-dependent energy equation was used to characterize the process of heat transfer during vitrification, as:

$$\frac{\partial T}{\partial t} = \alpha \nabla^2 T + \frac{\dot{\Phi}}{\rho c_p} \quad (10)$$

where T (K) is the temperature of droplet, t (s) is the cooling time, and α (m^2/s) is the thermal diffusivity, $\alpha = \lambda/\rho c_p$. ρ (kg/m^3) and c_p (kJ/(kg·K)) are the density and specific heat at constant pressure, and λ (W/(m·K)) is the thermal conductivity. $\dot{\Phi}$ (W/m^3) is the volumetric heat source as induced by latent heat (L(J/kg)) release during cooling.

Because the heat source $\left(\dot{\Phi}\right)$ stems from latent heat release due to ice formation, the amount of heat release (Φ (J/m^3) is related to the degree of ice crystallization. Thus,

$$\Phi = L \cdot \rho \cdot \chi \quad (11)$$

$$\dot{\Phi} = \frac{d\Phi}{dt} = L \cdot \rho \cdot \frac{d\chi}{dt} \quad (12)$$

Accordingly, Eq. (10) could be rewritten as:

$$\frac{\partial T}{\partial t} = \alpha \nabla^2 T + \frac{L}{c_p}\frac{d\chi}{dt} \quad (13)$$

Upon coupling with the diffusion process described by Eqs. (4), (5) and (7), Eq. (13) was written as:

$$\frac{\partial T}{\partial t} = \frac{(\lambda_{CPA} - \lambda_{cell})\frac{c_i}{c_0} + \lambda_{cell}}{((\rho_{CPA} - \rho_{cell})\frac{c_i}{c_0} + \rho_{cell})((c_{p,CPA} - c_{p,cell})\frac{c_i}{c_0} + c_{p,cell})}\nabla^2 T + \frac{(L_{CPA} - L_{cell})\frac{c_i}{c_0} + L_{cell}}{(c_{p,CPA} - c_{p,cell})\frac{c_i}{c_0} + c_{p,cell}}\frac{d\chi}{dt} \quad (14)$$

The two coupled equations, Eq. (9) and Eq. (14), were employed to show the coupled physical processes of vitrification. Note that latent heat was prescribed in the area of CPAs and inner cells, but not cell membranes for they are too thin to consider latent heat.

2.1.3. Boundary and initial conditions

When a droplet is dropped into liquid nitrogen, due to the Leidenfrost phenomenon, it will float and be covered by flowing nitrogen gas produced by vaporization of liquid nitrogen when the latent heat of droplet is releasing (Song et al., 2010). The surface of the droplet was thence set as convection boundary; further, because crystallization usually occurs below the melting temperature (T_m), the entire droplet was set at the melting temperature and hence crystallization was equal to zero at time 0, leading to:

$$\frac{\partial T}{\partial r} = \frac{h}{\lambda}(T - T_{LN}),\ r = R_0 \quad (15)$$

$$T = T_{m,i},\ t = 0 \quad (16)$$

$$\chi = 0,\ t = 0 \quad (17)$$

where r (m) is the radial coordinate, R_0 (m) is the radius of droplet encapsulating cell aggregate, T_{LN} (K) is the temperature of liquid nitrogen, and h ($W/(m^2 \cdot K)$) is the convective coefficient which considered the Leidenfrost phenomenon during direct cooling in liquid nitrogen (Heetae et al., 2011). We used the finite element (FE) method (COMSOL Multiphysics) to solve the above equations, with representative FE

meshes shown in Fig. 1**f**. The computational module of transient chemical diffusion was employed to calculate the CPA diffusion process, while the modules of transient heat transfer and partial differential equations were coupled and utilized to compute the cooling and crystallization. The relative tolerance of all computations was set as 1%. The sensitivity of FE meshes had been tested, which ensured a maximum error less than 1% if the mesh was further refined.

2.2. Experimental methods

To qualitatively verify the model, we experimentally vitrified cell-free droplets using droplet-based method and compared the measurement results with the numerical simulation results. Three different CPA concentration solutions (*i.e.*, water, 35% 1,2-propanediol + 65% water, and pure 1,2-propanediol) commonly used in biocryopreservation were prepared. The droplets were generated and injected in liquid nitrogen individually with manual micropipette. Droplets with a fixed volume of 10 μL (or, equivalently, a fixed diameter of 1.3 mm) were used. When the droplets were injected into liquid nitrogen, we observed that the droplets initially levitated as a result of the Leidenfrost phenomenon and then immerged in liquid nitrogen. After immerging, the droplets were immediately taken for imaging under a digital camera, from which the qualitative crystallization level could be visually observed by the transparent appearance of the frozen droplets. All experimental protocols were carried out in accordance with the guidelines, as approved by Xi'an Jiaotong University.

3. Results

For qualitative verification, we compared the experimental and simulation results of crystallization distribution in a 10-μL cell-free droplet for three different CPA concentration solutions, water, 35% 1,2-propanediol + 65% water, and pure 1,2-propanediol; Fig. 2. We observed that, with increasing concentration of 1, 2-propanediol, the transparency of vitrified droplet (*i.e.*, the representative of vitrification level) increased gradually (Fig. 2**a-c**), which agreed well with the simulation results for the decrease of crystallization (Fig. 2**d-f**). Since direct measurements of temperature and crystallization during ultrafast vitrification of microscale biomaterials are challenging, we compared the predicted temperature variation of a micrometer scale sample (~200 μm) using our model with existing computational data (Zhou et al., 2013). Also, we compared the predicted temperature variation of a millimeter scale (~1.5 mm) sample with existing experimental data (Teixeira et al., 2014). We noted that, at both the millimeter and micrometer scales, the temperature variation curves calculated by our model agreed well with existing studies (Fig. 2**g**), thus validating, at least qualitatively, the proposed numerical model.

To understand the physical processes in cell aggregates during droplet-based vitrification, we numerically vitrified a 200 μm droplet that encapsulated a 50 μm cell aggregate in liquid nitrogen and calculated the spatiotemporal evolution of its temperature and crystallization (Fig. 3). During cooling, the temperature of the droplet dramatically decreased to liquid nitrogen's temperature (77 K) in around 0.205 s, and formation of ice crystal occurred in the whole droplet. The maximum degree of crystallization, about 1.9×10^{-4} (Fig. 3**a**), appeared in the center of cell aggregate. This value agreed well with results in existing literatures (Choi and Bischof, 2010; Jiao et al., 2006) where the same order of crystallization was reported at similar characteristic length in cylindrical specimens. Further, the results of Fig. 3**a** indicated that, upon vitrification, the maximum crystallization in cell aggregates (*i.e.*, $\chi = 1.9 \times 10^{-4}$) was lower than the criterion of "innocuous" intracellular ice formation (*i.e.*, $\chi \leq 10^{-3}$) proposed by Karlsson et al. (1994), which means the degree of ice formation in cell aggregates is not harmful for cell. These results indicate that vitrification has been successfully achieved in the current droplet-based vitrification of cell aggregates. To further illustrate the variation of temperature and crystallization in cell aggregates, we calculated their temporal variations in the center of cell aggregate (Fig. 3**b**). We chose the center of cell aggregate because it possessed the highest temperature (also the lowest cooling rate) and the highest crystallization (Fig. 3**a**). We observed that the crystallization level increased dramatically during the initial stage of cooling, achieving soon a stable value. In contrast, the temperature monotonically decreased, faster at beginning and slower at last (Fig. 3**b**). Since the droplet surface was nearest to liquid nitrogen, it had a higher cooling rate than that at the center (Fig. 3**c**), thus could pass through the DTR much sooner, resulting in a much lower crystallization level on droplet surface (Fig. 3**d**).

In Fig. 3**b**, we drew a vertical arrow line from the stable point of the crystallization curve to the temperature curve to obtain the equivalent glass transition temperature (approximately 155 K) of the whole cell aggregate droplet on the temperature curve, which was higher than the glass transition temperature of water, 136 K (Ito et al., 1999). During

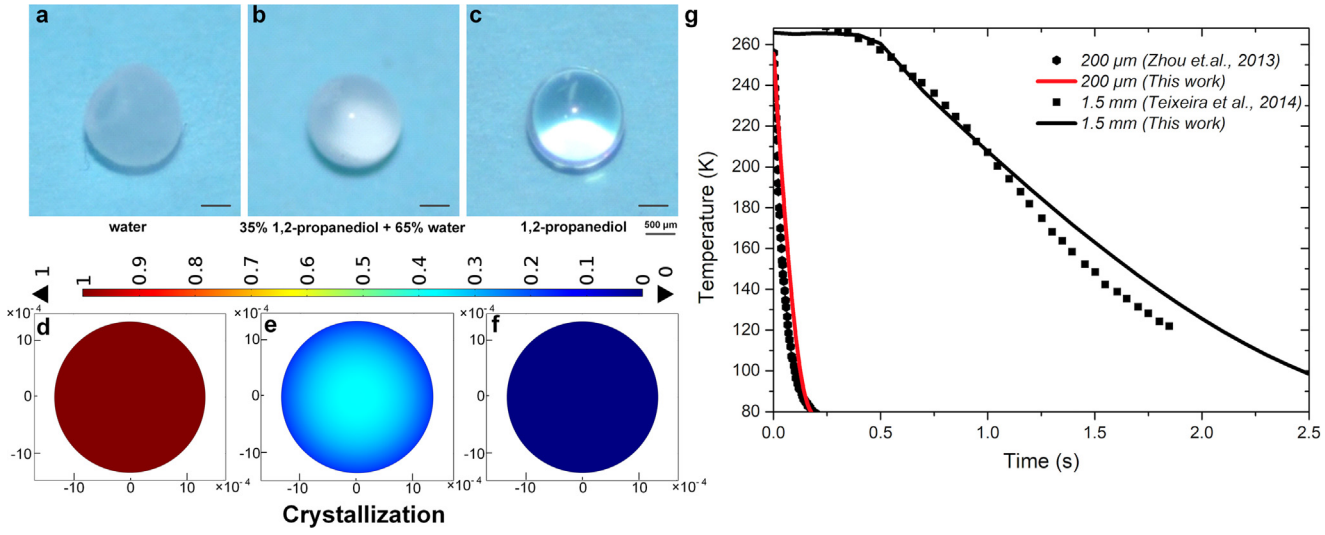

Fig. 2. Comparison of simulation results with qualitative experiments from this work and quantitative data from existing literature. Experimental pictures of 10 μL droplet after vitrfication: (a) water, (b) 35% 1,2-propanediol + 65% water, and (c) pure 1,2-propanediol droplets after cooling in liquid nitrogen using the droplet-based method; (d), (e), and (f) were numerical simulation results of crystallization distribution of 10 μL water, 35% 1,2-propanediol + 65% water, and pure 1,2-propanediol droplets, respectively; (g) Comparison of calculated results from this work with quantitative data from existing literature.

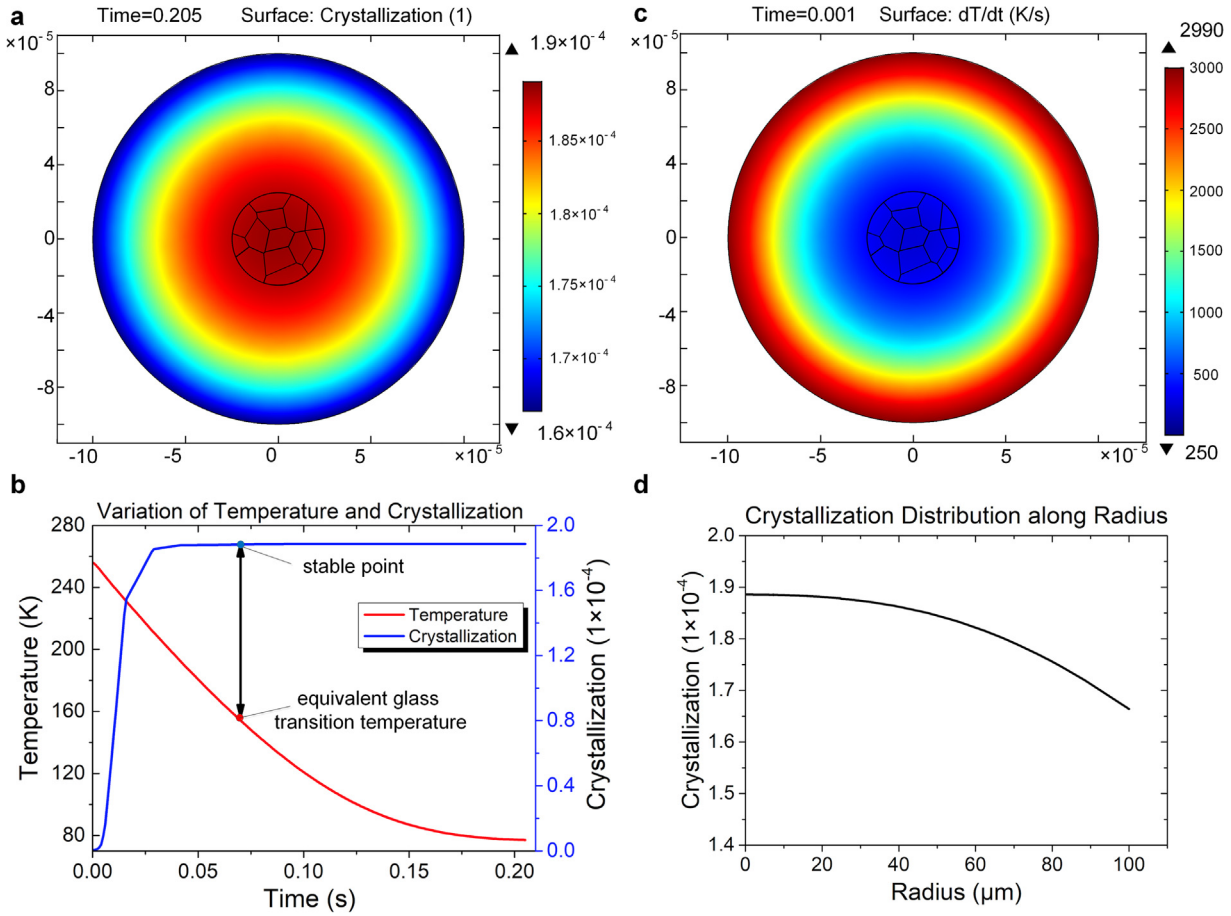

Fig. 3. Spatial and temporal distributions of temperature and crystallization in cell aggregate encapsulating droplet during vitrification. (a) Final distribution of crystallization; (b) Variation of temperature and crystallization with time; (c) Initial distribution of cooling rate in droplet; (d) Final crystallization distribution along radius of droplet.

vitrification, if the temperature of cell aggregate decreases to this equivalent glass transition temperature, the crystallization process can be considered as completed, *i.e.*, the glass transition process is completed. Also, this method can be used to estimate the equivalent glass transition temperature of cell aggregate droplets having even more complex structures. The equivalent glass transition temperature can be used to guide the experimental design of vitrification cryopreservation, so as to improve the cooling rate between melting temperature and equivalent glass transition temperature to achieve high vitrification level (*i.e.*, low crystallization level).

To further simulate the vitrification process in cell aggregates, we considered the effect of cell membrane. It is worth mentioning that conflicting results of cell membrane effect on heat transfer had been reported: some studies stated that there was a thermal gradient in cell membrane resulting in temperature difference between extra and inner parts of cells, while others conjectured that the thermal effect of cell membrane was negligible due to its small thickness (Rabin, 2002; Vincze et al., 2005). Our simulation results showed that, relative to the case without considering cell membrane, the presence of cell membrane could only induce a 0.69% difference in the maximum degree of crystallization at the end of cooling (Fig. 4, $\lambda/\lambda_0 = 1$ and without membrane). Further, as information regarding the accurate thermal conductivity of cell membrane was lacking, we changed its thermal conductivity across four orders of magnitude. Nonetheless, the biggest difference achieved in the maximum degree of crystallization in cell aggregates was less than 2×10^{-6} (*i.e.*, only a 1.0% difference) (Fig. 4, $\lambda/\lambda_0 = 0.1, 1, 10, 100$). Overall, the present results suggested that cell membrane had no significant heat transfer effect on crystallization

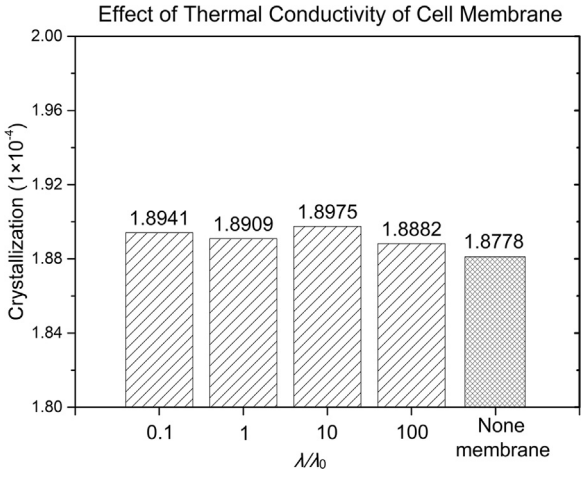

Fig. 4. Effect of cell membrane thermal conductivity on maximum crystallization in cell aggregate encapsulating droplet.

level, even if the non-dimensional thermal conductivity of cell membrane was increased from 0.1 to 100. This was mainly attributed to the ultra-thin thickness of cell membrane (~ 10 nm) compared to cell diameter (~ 10 μm) (Korn, 1966) and hence its ignorable heat resistance.

Although cell membrane has negligible effects on the cooling process of cell aggregates, it may have significant effects on the mass transfer of CPA before vitrification due to permselectivity of biologic

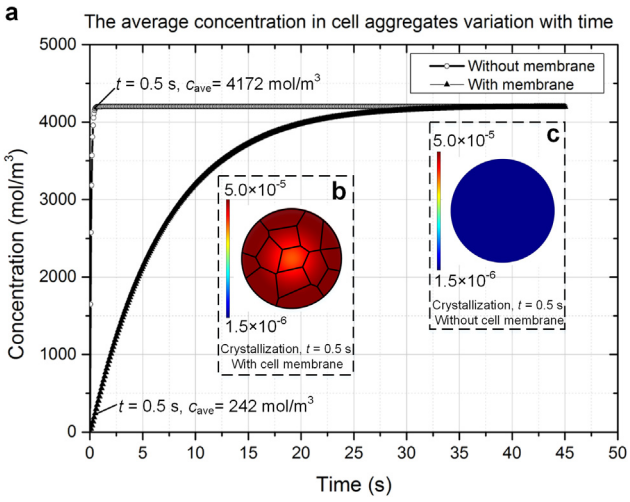

Fig. 5. Effect of cell membrane on CPA diffusion. (a) Temporal variation of average concentration in 50 μm cell aggregate (White point: without cell membrane; Black point: with cell membrane); Crystallization in cell aggregates: (b) Effect of cell membrane accounted for (after 0.5 s exposing in CPA, followed by vitrification); (c) Effect of cell membrane neglected (after 0.5 s exposing in CPA, followed by vitrification).

membranes (Stewart, 1998). To study the mass transfer effect of cell membrane and the mass transfer (diffusion) process of CPA in cell aggregates, cases both considering cell membrane (black points in Fig. 5**a**) and ignoring cell membrane (white points in Fig. 5**a**) were calculated. The entire diffusion process of CPA in a 50 μm cell aggregate took 45 s when considering cell membrane and 0.75 s when ignoring the cell membrane. In other words, for the CPA concentration to reach steady state, a 50 μm cell aggregate with cell membrane would take almost 60 times longer than that without cell membrane (Fig. 5**a**). Thus, at the same time point of CPA diffusion, for example 0.5 s (Fig. 5**a**), the CPA concentration exhibited marked difference between cell aggregates with and without cell membrane, 242 mol/m^3 as *versus* 4172 mol/m^3. This induced difference in thermal properties of cell aggregates, thus affecting subsequent cooling and final crystallization. For instance, at the 0.5 s of CPA diffusion, the cell aggregates with cell membrane (5.0×10^{-5}) achieved much higher crystallization (Fig. 5**b**) than those without cell membrane (1.9×10^{-6}) (Fig. 5**c**) after vitrification. Therefore, cell membrane may be treated as a barrier for CPA diffusion in cell aggregates and, in this way, cell membrane will affect the final crystallization level of cell aggregates upon cooling.

However, even if cell membrane may act as a barrier of CPA diffusion, this does not mean a longer CPA loading is better. If cell aggregates are exposed in CPA excessively during the diffusion process, excessive CPA may diffuse across cell membrane into cells and hence cause cell damage due to the toxicity of CPA as induced by osmotic shock (Fahy, 2010). This suggests that there exists an optimized CPA loading time for cell aggregates, where a too-long CPA loading causes reduced crystal formation, but at the price of CPA toxicity-induced cell damage. To explore the effect of CPA loading time for cell aggregates cryopreservation, we exposed a 50 μm cell aggregate in CPA for different time durations and calculated the variation of CPA concentration after CPA loading and homologous crystallization after cooling, with the effect of cell membrane on CPA diffusion accounted for (Fig. 6). Representatively, the exposure time points were chosen at $t = 0.0$ s, 5.0 s, 45.0 s when the average concentration in the cell aggregate reached 0, half of surrounding concentration ($c_{.5}$), and surrounding concentration (c_0) (Fig. 6**b**). The results indicated that CPA concentration in cell aggregates increased with exposure time in CPA solution while crystallization decreased remarkably with increasing concentration. In addition, the crystallization level of cell aggregates decreased sharply during the initial stage of CPA diffusion, but then decreased

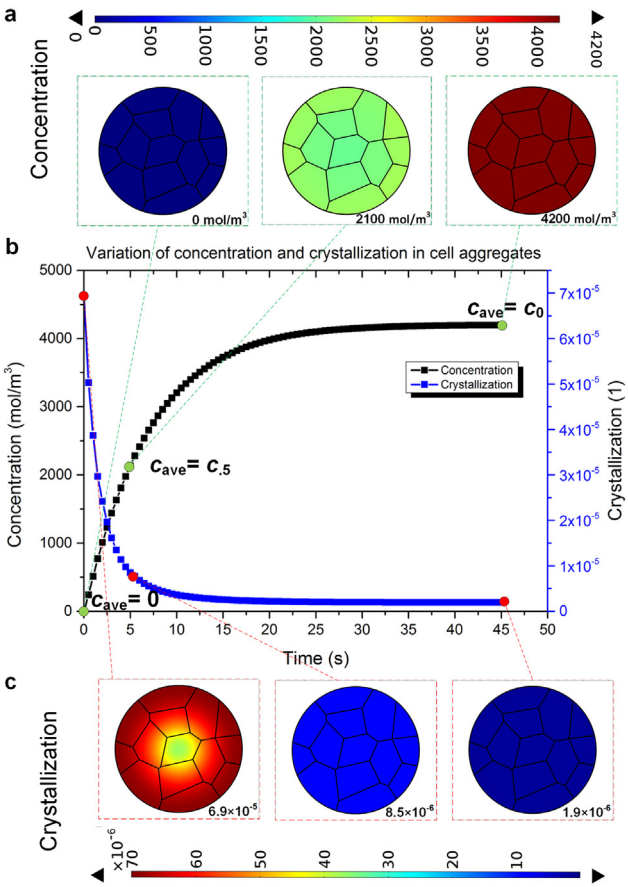

Fig. 6. Effect of CPA diffusion on crystallization in cell aggregate after vitrification. (a) Concentration distribution in cell aggregate when $c_{ave} = 0$, $c_{.5}$, c_0; (b) Variation of CPA diffusion and crystallization in 50 μm cell aggregate with cell membrane (Black line: Average concentration in cell aggregate; Blue line: Maximum crystallization in cell aggregate); (c) Crystallization distribution in cell aggregate when $c_{ave} = 0$, $c_{.5}$, c_0.

much slowly during subsequent diffusion (Fig. 6**b**). It could be seen from Fig. 6**a** and **c** that, initially, as there existed none CPA in the cell aggregate, the highest crystallization level was reached (6.9×10^{-5}). At the time of 5 s, the CPA concentration in cell aggregate arrived at 2100 mol/m^3, reducing the crystallization to 8.5×10^{-6}. Eventually (45 s), the concentration reached 4200 mol/m^3, and the crystallization dropped to 1.9×10^{-6}. That is, the initial 11% time of CPA diffusion (5 s) induced a 90% decrease in crystallization level (6.0×10^{-5}). This demonstrated that effective protection of CPA on vitrification mainly occurred during the initial stage of CPA diffusion, thus a longer CPA loading does not necessarily bring effective decrease in crystallization but may bring more toxicity of CPA to cells. This finding reveals the importance of cell membrane in CPA diffusion, which could be a guidance to design the optimal CPA loading approaches. For perspective, if the permselectivity of cell membranes could be turned *via* certain drugs, the CPA diffusion process might be accelerated thus to avoid the long-term exposure of cells in CPA.

The diameter of cell aggregates is another important factor in vitrification of cell aggregates encapsulated in droplets, which may affect heat and mass transfer. To illustrate this, we simulated aggregates with three different cell aggregate diameters, 50 μm, 100 μm, and 150 μm, to show the relationship between diameter and crystallization (Fig. 7). We observed that the crystallization level increased significantly with increasing diameter of cell aggregates. For heat transfer, a larger cell aggregate means it needs more time to exchange heat flux with liquid nitrogen, and the total latent heat will increase. Thus, it will cost more time to complete the cooling process and the final crystallization level

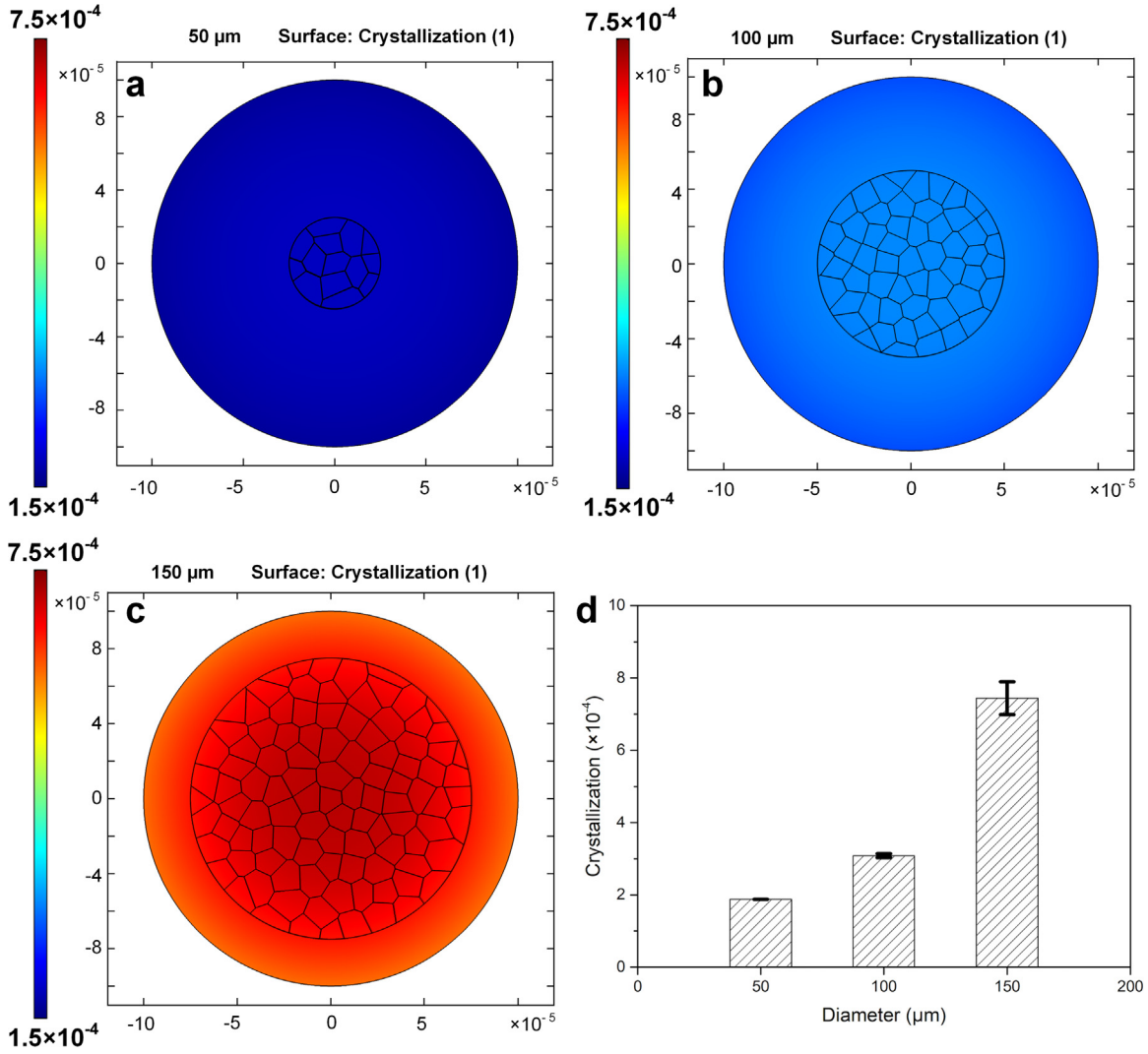

Fig. 7. Effect of cell aggregate diameter on crystallization after vitrification. Cloud figures (a), (b), (c) were final crystallization distribution in different cell aggregates (50 μm, 100 μm, 150 μm) encapsulated in droplets (200 μm); (d) Shadow bars were maximum crystallization in cell aggregates with different diameters encapsulated in droplets, and the error bars (at the top of shadow bars) were calculated using three different initial random topologies for each cell aggregate.

will increase. For mass transfer, because cell membrane is a diffusional resistance of CPA loading, a larger cell aggregate will take longer time for CPA to diffuse into the entire aggregate. Thus, CPA concentration would be lower in the inner part of the larger cell aggregate, resulting in higher crystallization levels. At the same time, even if the diameter was increased to as large as 150 μm, there was still very low crystallization in the cell aggregate (7.2×10^{-4}), as shown in Fig. 7**c**. This demonstrated that the droplet-based vitrification method has potential in cryopreserving larger cell aggregates. To evaluate the effect of initial random topology, we calculated the droplet based vitrification process of each cell aggregate using three different initial topologies, and compared the resulting crystallization in the cell aggregate. We found that, the initial topology does not affect significantly droplet vitrification of cell aggregate, as reflected by the error bars in Fig. 7**d**. The reason is that, even if the initial topologies chosen are somewhat different, the average diameters of the cells are similar, and the diameters of cell aggregates and the encapsulated droplet are fixed. This implies that the cooling boundary conditions, heat capacity and latent heat of the entire system are similar, and hence the heat transfer and crystallization processes are not significantly affected by the initial random topologies. However, the effect of initial random topology becomes relatively larger in larger cell aggregate, which attributes to the increasing uncertainty of cell aggregates inner structures leading the slight difference of heat transfer and crystallization processes.

4. Discussion

Through numerical investigation of the droplet vitrification of cell aggregates, we found that although cell membrane is not an obvious barrier in heat transfer, it affects the diffusion of CPA remarkably as a biologic film and hence the subsequent crystallization in cell aggregates. Heat transfer in cell aggregates is dominated by conductive heat transfer (Song et al., 2010). The thermal effect of each domain is determined by its thermal barrier ($R_T = \delta/k$, where R_T is the thermal barrier, δ is the thickness and k is the thermal conductivity). Since cell membrane is very thin (~10 nm) (Korn, 1966), the corresponding thermal barrier is very small. Therefore, cell membrane has negligible effect on heat transfer during vitrification. However, since the cell membrane is a biologic membrane having permselectivity of molecules (Lieb and Stein, 1972; Stewart, 1998), the diffusion of cryoprotectant in cell membrane is much harder than in the inner part of cell ($D_{mem} \ll D_{cell}$, where D_{mem} and D_{cell} are the diffusivity in cell membrane and inner cell

respectively). Thus, as cell membrane can be treated as a barrier for cryoprotectant in cell aggregates, it plays a large role in the mass transfer process of cell aggregates and thus affects the vitrification of cell aggregates.

It is worth mentioning that, the mass transfer process during CPA loading had been extensively studied (Devireddy, 2005; Devireddy et al., 2002; Kleinhans, 1998; Scherr et al., 2012). One of the representative theory was the Kedem–Katchalskymembrane permeability model (Kleinhans, 1998), which illustrated the two simultaneous processes of water dehydration and CPA permeation. This two parameters model was more accurate for cells as it had considered volume shrinking of cells. However, for large tissues, the volume shrinking of cells was limited by the large structure of tissues, and the dominant mass transfer from boundary to center of large tissues was caused by chemical gradient. Besides, another model of chemical molecules diffusion was commonly utilized to illustrate CPA loading of large tissues (Lawson et al., 2012; Lee and Rubinsky, 1989), since CPA loading into large biomaterials was mainly driven by chemical gradient. While advanced models coupling these two models were developed to illustrate the multiscale mass transfer process (Shaik and Devireddy, 2017), in the present work, we adopted the chemical molecules diffusion model as a first attempt to understand the dominant physical processes occurring during cell aggregate vitrification.

Further, the vitrification of cell aggregates contains more complex physics than we currently reached, which is influenced by many factors, such as cell type, kind of CPA, compact degree of cell aggregates, dehydration of cell aggregates during CPA loading and cooling, location of cell aggregates in droplet, *etc.* Furthermore, the amount, topology and thermal properties of cell inner structures (*e.g.,* cell cytoskeleton), and the mechanical deformation of cell and cell membrane during cooling and crystallization may also affect cell aggregate vitrification (Clark and Paluch, 2011; Vernerey and Farsad, 2011). For instance, since cell cytoskeleton may have different thermal properties from intracellular liquids (ElAfandy et al., 2017), the amount and topology will affect the thermal properties of cells used in the current model. Probably a porous media model could be engaged to calculate the equivalent thermal properties of cells and cell aggregate before simulating the vitrification process (Feng et al., 2015). It is worth mentioning that, a recent study indicated the interfacial water near cell membrane could play an important role in thermal dissipation of cells (Wang et al., 2016), and it might also influence the heat transfer process during cooling. Therefore, the factors discussed above may all potentially affect the vitrification process of cell aggregates. To address these issues, more advanced model(s) will be used in future studies to improve our theory.

5. Conclusion

Droplet-based vitrification of cell aggregates had been investigated using the method of finite elements. Based on the polygon shaped morphology of cell aggregates, a voronoi geometry model of cell aggregates was established, with the effect of cell membrane accounted for. The governing equations of diffusion, heat transfer and crystallization were coupled to quantify the variation and distribution of concentration (CPA), temperature and crystallization during vitrification of cell aggregates.

It was demonstrated that high degree of vitrification (*i.e.*, low degree of crystallization) could be achieved during cryopreservation of cell aggregates by using droplet-based vitrification. In the cell aggregates droplet, the crystallization level increased dramatically during the initial stage of cooling, achieving fast its stable value. Since the droplet boundary was nearest to liquid nitrogen thus exhibited a higher cooling rate, it had a lower crystallization level relative to the droplet center. The equivalent glass transition temperature was defined to characterize cell aggregate vitrification, which can experimentally guide vitrification cryopreservation.

Cell membrane played an important role in cell aggregate vitrification. During cooling, cell membrane may not be an obvious barrier for heat transfer but will affect the diffusion of CPA and thus the final crystallization of cell aggregates. The effective protection of CPA on vitrification occurred during the initial stage of CPA diffusion, and a longer CPA loading process does not necessarily lead to effective drop in crystallization but rather may induce more toxicity of CPA to cell aggregates.

Due to increased transfer distances of diffusion and heat, the crystallization level increased with the diameter of aggregates in droplet of fixed size. However, even if the diameter was increased to as large as 150 μm, there was still very low crystallization in cell aggregate. This demonstrated that the droplet-based vitrification method has significant potential in cryopreserving larger cell aggregates.

Acknowledgement

This work was financially supported by the National Natural Science Foundation of China (11522219, 11532009, 51676156, 81401270). S.F. was also supported by the Postdoctoral Science Foundation of China (2016M590942). C.J. was also supported by the Natural Science Basic Research Plan in Shaanxi Province of China (2016JM8120).

Author contributions

M.S. and F.X. designed the simulations, while M.S. and T.J.L. designed the experiments. M.S. performed the simulations and experiments and analyzed the data. S.F., X.Z. and C.J. contributed instruments and materials. M.S. wrote the manuscript while S.F., X.Z., C.J., F.X. and T.J.L. revised the manuscript.

Additional information

The authors declare no conflict of interest.

References

An, L., Chang, S., Hu, Y., Li, Y., Xu, B., Zhang, F., Yang, L., Presicce, G.A., Du, F., 2015. Efficient cryopreservation of mouse embryos by modified droplet vitrification (MDV). Cryobiology 71, 70–76. http://dx.doi.org/10.1016/j.cryobiol.2015.05.067.

Asghar, W., El Assal, R., Shafiee, H., Pitteri, S., Paulmurugan, R., Demirci, U., 2015. Engineering cancer microenvironments for in vitro 3-D tumor models. Mater. Today 18, 539–553. http://dx.doi.org/10.1016/j.mattod.2015.05.002.

Boutron, P., 1986. Comparison with the theory of the kinetics and extent of ice crystallization and of the glass-forming tendency in aqueous cryoprotective solutions. Cryobiology 23, 88–102. http://dx.doi.org/10.1016/0011-2240(86)90022-2.

Boutron, P., Mehl, P., 1990. Theoretical prediction of devitrification tendency: determination of critical warming rates without using finite expansions. Cryobiology 27, 359–377. http://dx.doi.org/10.1016/0011-2240(90)90015-V.

Bowman, H.F., Cravalho, E.G., Woods, M., 1975. Theory, measurement, and application of thermal properties of biomaterials. Annu. Rev. Biophys. Bioeng. 4, 43–80. http://dx.doi.org/10.1146/annurev.bb.04.060175.000355.

Chan, H.F., Zhang, Y., Ho, Y.-P., Chiu, Y.-L., Jung, Y., Leong, K.W., 2013. Rapid formation of multicellular spheroids in double-emulsion droplets with controllable microenvironment. Sci. Rep. 3, 3462. http://dx.doi.org/10.1038/srep03462.

Choi, J., Bischof, J.C., 2010. Review of biomaterial thermal property measurements in the cryogenic regime and their use for prediction of equilibrium and non-equilibrium freezing applications in cryobiology. Cryobiology 60, 52–70. http://dx.doi.org/10.1016/j.cryobiol.2009.11.004.

Clark, A.G., Paluch, E., 2011. Mechanics and regulation of cell shape during the cell cycle. Cell Cycle Dev. 31–73. Springer. https://doi.org/10.1007/978-3-642-19065-0_3.

da Fonseca Cardoso, L.M., Pinto, M.A., Pons, A.H., Alves, L.A., 2017. Cryopreservation of rat hepatocytes with disaccharides for cell therapy. Cryobiology 78, 15–21. http://dx.doi.org/10.1016/j.cryobiol.2017.07.010.

Demirci, U., Montesano, G., 2007. Cell encapsulating droplet vitrification. Lab Chip 7, 1428–1433. http://dx.doi.org/10.1039/B705809H.

Devireddy, R.V., 2005. Predicted permeability parameters of human ovarian tissue cells to various cryoprotectants and water. Mol. Reprod. Dev. 70, 333–343. http://dx.doi.org/10.1002/mrd.20209.

Devireddy, R.V., Smith, D.J., Bischof, J.C., 2002. Effect of microscale mass transport and phase change on numerical prediction of freezing in biological tissues. J. Heat. Transf. 124, 365. http://dx.doi.org/10.1002/mrd.20209.

Dhali, A., Anchamparuthy, V., Butler, S., Pearson, R., Mullarky, I., Gwazdauskas, F., 2009. Effect of droplet vitrification on development competence, actin cytoskeletal integrity and gene expression in in vitro cultured mouse embryos. Theriogenology 71, 1408–1416. http://dx.doi.org/10.1016/j.theriogenology.2009.01.011.

Dou, R., Saunders, R.E., Mohamet, L., Ward, C.M., Derby, B., 2015. High throughput cryopreservation of cells by rapid freezing of sub-μL drops using inkjet printing--cryoprinting. Lab Chip 15, 3503–3513. http://dx.doi.org/10.1039/C5LC00674K.
El Assal, R., Guven, S., Gurkan, U.A., Gozen, I., Shafiee, H., Dalbeyler, S., Abdalla, N., Thomas, G., Fuld, W., Illigens, B.M., 2014. Bio-inspired cryo-ink preserves red blood cell phenotype and function during nanoliter vitrification. Adv. Mater. 26, 5815–5822. http://dx.doi.org/10.1002/adma.201400941.
ElAfandy, R.T., AbuElela, A.F., Mishra, P., Janjua, B., Oubei, H.M., Büttner, U., Majid, M.A., Ng, T.K., Merzaban, J.S., Ooi, B.S., 2017. Nanomembrane-based, thermal--transport biosensor for living cells. Small 13, 1603080. http://dx.doi.org/10.1002/smll.201603080.
Ewald, A.J., 2017. Pulling cells out of tumours. Nat. Cell Biol. 19, 147–149. http://dx.doi.org/10.1038/ncb3484.
Fahy, G.M., 2010. Cryoprotectant toxicity neutralization. Cryobiology 60, S45–S53. http://dx.doi.org/10.1016/j.cryobiol.2009.05.005.
Fan, Y.T., Nguyen, D.T., Akay, Y., Xu, F., Akay, M., 2016. Engineering a brain cancer chip for high-throughput drug screening. Sci. Rep. 6, 25062. http://dx.doi.org/10.1038/srep25062.
Feng, S., Zhang, Y., Shi, M., Wen, T., Lu, T.J., 2015. Unidirectional freezing of phase change materials saturated in open-cell metal foams. Appl. Therm. Eng. 88, 315–321. http://dx.doi.org/10.1016/j.applthermaleng.2014.09.055.
Fierro-González, J.C., White, M.D., Silva, J.C., Plachta, N., 2013. Cadherin-dependent filopodia control preimplantation embryo compaction. Nat. Cell Biol. 15, 1424–1433. http://dx.doi.org/10.1038/ncb2875.
Flick, E.W., 1998. Industrial Solvents Handbook, 5th ed. Noyes Data Corp., Westwood, N.J.
Florczyk, S.J., Liu, G., Kievit, F.M., Lewis, A.M., Wu, J.D., Zhang, M., 2012. 3D porous chitosan-alginate scaffolds: a new matrix for studying prostate cancer cell-lymphocyte interactions in vitro. . Adv. Healthc. Mater. 1, 590–599. http://dx.doi.org/10.1002/adhm.201100054.
Friedrich, J., Seidel, C., Ebner, R., Kunz-Schughart, L.A., 2009. Spheroid-based drug screen: considerations and practical approach. Nat. Protoc. 4, 309–324. http://dx.doi.org/10.1038/nprot.2008.226.
Gao, B., Yang, Q., Zhao, X., Jin, G., Ma, Y., Xu, F., 2016. 4D bioprinting for biomedical applications. Trends Biotechnol. 34, 746–756. http://dx.doi.org/10.1016/j.tibtech.2016.03.004.
Giwa, S., Lewis, J.K., Alvarez, L., Langer, R., Roth, A.E., Church, G.M., Markmann, J.F., Sachs, D.H., Chandraker, A., Wertheim, J.A., Rothblatt, M., Boyden, E.S., Eidbo, E., Lee, W.P.A., Pomahac, B., Brandacher, G., Weinstock, D.M., Elliott, G., Nelson, D., Acker, J.P., Uygun, K., Schmalz, B., Weegman, B.P., Tocchio, A., Fahy, G.M., Storey, K.B., Rubinsky, B., Bischof, J., Elliott, J.A.W., Woodruff, T.K., Morris, G.J., Demirci, U., Brockbank, K.G.M., Woods, E.J., Ben, R.N., Baust, J.G., Gao, D.Y., Fuller, B., Rabin, Y., Kravitz, D.C., Taylor, M.J., Toner, M., 2017. The promise of organ and tissue preservation to transform medicine. Nat. Biotechnol. 35, 530–542. http://dx.doi.org/10.1038/nbt.3889.
Hamilton, G., 1998. Investigations of the Thermal Properties of Human and Animal Tissues. University of Glasgow.
Heetae, K., Young, H.L., Hoonyoung, C., 2011. Levitation time measurement of water drops on the surface of liquid nitrogen. J. Korean Phys. Soc. 58, 1628. http://dx.doi.org/10.3938/jkps.58.1628.
Isachenko, E., Isachenko, V., Katkov, I.I., Rahimi, G., Schöndorf, T., Mallmann, P., Dessole, S., Nawroth, F., 2004. DNA integrity and motility of human spermatozoa after standard slow freezing versus cryoprotectant-free vitrification. Hum. Reprod. 19, 932–939. http://dx.doi.org/10.1093/humrep/deh194.
Ito, K., Moynihan, C.T., Angell, C.A., 1999. Thermodynamic determination of fragility in liquids and a fragile-to-strong liquid transition in water. Nature 398, 492–495. http://dx.doi.org/10.1038/19042.
Jabrane, S., Letoffe, J., Claudy, P., 1995. Vitrification and crystallization in the R (−) 1, 2-propanediol-S (+) 1, 2-propanediol system. Thermochim. Acta 258, 33–47. http://dx.doi.org/10.1016/0040-6031(94)02235-G.
Jiao, A., Han, X., Critser, J.K., Ma, H., 2006. Numerical investigations of transient heat transfer characteristics and vitrification tendencies in ultra-fast cell cooling processes. Cryobiology 52, 386–392. http://dx.doi.org/10.1016/j.cryobiol.2006.01.009.
Karlsson, J.O.M., Cravalho, E.G., Toner, M., 1994. A model of diffusion-limited ice growth inside biological cells during freezing. J. Appl. Phys. 75, 4442. http://dx.doi.org/10.1063/1.355959.
Khosla, K., Wang, Y.R., Hagedorn, M., Qin, Z.P., Bischof, J., 2017. Gold nanorod induced warming of embryos from the cryogenic state enhances viability. ACS Nano 11, 7869–7878. http://dx.doi.org/10.1021/acsnano.7b02216.
Kleinhans, F., 1998. Membrane permeability modeling: Kedem–Katchalsky vs a two-parameter formalism. Cryobiology 37, 271–289. http://dx.doi.org/10.1006/cryo.1998.2135.
Korn, E.D., 1966. Structure of biological membranes. Science 153, 1491–1498.
Krieg, M., Arboleda-Estudillo, Y., Puech, P.-H., Käfer, J., Graner, F., Müller, D., Heisenberg, C.-P., 2008. Tensile forces govern germ-layer organization in zebrafish. Nat. Cell Biol. 10, 429–436. http://dx.doi.org/10.1126/science.153.3743.1491.
Kuleshova, L., Gouk, S., Hutmacher, D., 2007. Vitrification as a prospect for cryopreservation of tissue-engineered constructs. Biomaterials 28, 1585–1596. http://dx.doi.org/10.1016/j.biomaterials.2006.11.047.
Lawson, A., Mukherjee, I.N., Sambanis, A., 2012. Mathematical modeling of cryoprotectant addition and removal for the cryopreservation of engineered or natural tissues. Cryobiology 64, 1–11. http://dx.doi.org/10.1016/j.cryobiol.2011.11.006.
Lecuit, T., Lenne, P.F., 2007. Cell surface mechanics and the control of cell shape, tissue patterns and morphogenesis. Nat. Rev. Mol. Cell Biol. 8, 633–644. http://dx.doi.org/10.1038/nrm2222.
Lee, C.Y., Rubinsky, B., 1989. A multi-dimensional model of momentum and mass transfer in the liver. Int. J. Heat. Mass Transf. 32, 2421–2434. http://dx.doi.org/10.1016/0017-9310(89)90202-0.
Li, Y., Tan, J.C., Li, L.S., 2010. Comparison of three methods for cryopreservation of human embryonic stem cells. Fertil. Steril. 93, 999–1005. http://dx.doi.org/10.1016/j.fertnstert.2008.10.052.
Lieb, W., Stein, W., 1972. The molecular basis of simple diffusion within biological membranes. Curr. Top. Membr. Trans. 2, 1–39. http://dx.doi.org/10.1016/S0070-2161(08)60340-8.
Ma, H., Marti-Gutierrez, N., Park, S.W., Wu, J., Lee, Y., Suzuki, K., Koski, A., Ji, D.M., Hayama, T., Ahmed, R., Darby, H., Van Dyken, C., Li, Y., Kang, E., Park, A.R., Kim, D., Kim, S.T., Gong, J.H., Gu, Y., Xu, X., Battaglia, D., Krieg, S.A., Lee, D.M., Wu, D.H., Wolf, D.P., Heitner, S.B., Belmonte, J.C.I., Mato, P.A., Kim, J.S., Kaul, S., Mitalipov, S., 2017. Correction of a pathogenic gene mutation in human embryos. Nature 548, 413–419. http://dx.doi.org/10.1038/nature23305.
Magalhães, R., Nugraha, B., Pervaiz, S., Yu, H., Kuleshova, L.L., 2012. Influence of cell culture configuration on the post-cryopreservation viability of primary rat hepatocytes. Biomaterials 33, 88–95. http://dx.doi.org/10.1016/j.biomaterials.2011.10.015.
Manning, M.L., Foty, R.A., Steinberg, M.S., Schoetz, E.-M., 2010. Coaction of intercellular adhesion and cortical tension specifies tissue surface tension. Proc. Natl. Acad. Sci. Usa. 107, 12517–12522. http://dx.doi.org/10.1073/pnas.1003743107.
Manuchehrabadi, N., Gao, Z., Zhang, J.J., Ring, H.L., Shao, Q., Liu, F., McDermott, M., Fok, A., Rabin, Y., Brockbank, K.G.M., Garwood, M., Haynes, C.L., Bischof, J.C., 2017. Improved tissue cryopreservation using inductive heating of magnetic nanoparticles. Sci. Transl. Med. 9, eaah4586. http://dx.doi.org/10.1126/scitranslmed.aah4586.
Martin, M., Annamalai, K., Claridge, D., 1999. The effects of glycol addition to a static-water-cooled thermal energy storage system. In: Proceedings of the renewable and advanced energy systems for the 21st Century, Maui, HI (US), April 11-15.
Park, B.K., Yi, N., Park, J., Kim, D., 2013. Thermal conductivity of single biological cells and relation with cell viability. Appl. Phys. Lett. 102, 203702. http://dx.doi.org/10.1063/1.4807471.
Pedersen, P.S., Holstein-Rathlou, N.H., Larsen, P.L., Qvortrup, K., Frederiksen, O., 1999. Fluid absorption related to ion transport in human airway epithelial spheroids. Am. J. Physiol. Lung Cell Mol. Physiol. 277, L1096–L1103. http://dx.doi.org/10.1152/ajplung.1999.277.6.L1096.
Rabin, Y., 2002. Is intracellular hyperthermia superior to extracellular hyperthermia in the thermal sense? Int. J. Hyperth. 18, 194–202. http://dx.doi.org/10.1080/02656730110116713.
Rawal, S., Harrington, S., Williams, S.J., Ramachandran, K., Stehno-Bittel, L., 2017. Long-term cryopreservation of reaggregated pancreatic islets resulting in successful transplantation in rats. Cryobiology 76, 41–50. http://dx.doi.org/10.1016/j.cryobiol.2017.04.010.
Ryoun Youn, J., Seok Song, Y., 2012. Cell-encapsulating droplet formation and freezing. Appl. Phys. Lett. 101, 133701. http://dx.doi.org/10.1063/1.4754611.
Sansinena, M., Santos, M., Zaritzky, N., Chirife, J., 2011. Numerical simulation of cooling rates in vitrification systems used for oocyte cryopreservation. Cryobiology 63, 32–37. http://dx.doi.org/10.1016/j.cryobiol.2011.04.006.
Scherr, T., Quitadamo, C., Tesvich, P., Park, D.S.-W., Tiersch, T., Hayes, D., Choi, J.-W., Nandakumar, K., Monroe, W.T., 2012. A planar microfluidic mixer based on logarithmic spirals. J. Micromech. Microeng. 22, 055019. http://dx.doi.org/10.1088/0960-1317/22/5/055019.
Seo, M., Jeong, S., 2010. Analysis of self-pressurization phenomenon of cryogenic fluid storage tank with thermal diffusion model. Cryogenics 50, 549–555. http://dx.doi.org/10.1016/j.cryogenics.2010.02.021.
Shaik, S.M., Devireddy, R.V., 2017. Heat and Mass Transfer Models and Measurements for Low-Temperature Storage of Biological Systems. Handbook of Thermal Science and Engineering. pp. 1–39. http://dx.doi.org/10.1007/978-3-319-32003-8_73-1.
Shi, M., Ling, K., Yong, K.W., Li, Y., Feng, S., Zhang, X., Pingguan-Murphy, B., Lu, T.J., Xu, F., 2015. High-throughput non-contact vitrification of cell-laden droplets based on cell printing. Sci. Rep. 5, 17928. http://dx.doi.org/10.1038/srep17928.
Skardal, A., Murphy, S.V., Devarasetty, M., Mead, I., Kang, H.-W., Seol, Y.-J., Zhang, Y.S., Shin, S.-R., Zhao, L., Aleman, J., 2017. Multi-tissue interactions in an integrated three-tissue organ-on-a-chip platform. Sci. Rep. 7, 8837. http://dx.doi.org/10.1038/s41598-017-08879-x.
Song, Y.S., Adler, D., Xu, F., Kayaalp, E., Nureddin, A., Anchan, R.M., Maas, R.L., Demirci, U., 2010. Vitrification and levitation of a liquid droplet on liquid nitrogen. Proc. Natl. Acad. Sci. USA 107, 4596–4600. http://dx.doi.org/10.1073/pnas.0914059107.
Souza, G.R., Molina, J.R., Raphael, R.M., Ozawa, M.G., Stark, D.J., Levin, C.S., Bronk, L.F., Ananta, J.S., Mandelin, J., Georgescu, M.-M., 2010. Three-dimensional tissue culture based on magnetic cell levitation. Nat. Nanotechnol. 5, 291–296. http://dx.doi.org/10.1038/nnano.2010.23.
Stewart, P.S., 1998. A review of experimental measurements of effective diffusive permeabilities and effective diffusion coefficients in biofilms. Biotechnol. Bioeng. 59, 261–272. http://dx.doi.org/10.1002/(SICI)1097-0290(19980805)59:3<261::AID-BIT1>3.0.CO;2-9.
Takagi, R., Ishimaru, J., Sugawara, A., Toyoshima, K.-e., Ishida, K., Ogawa, M., Sakakibara, K., Asakawa, K., Kashiwakura, A., Oshima, M., 2016. Bioengineering a 3D integumentary organ system from iPS cells using an in vivo transplantation model. Sci. Adv. 2, e1500887. http://dx.doi.org/10.1126/sciadv.1500887.
Teixeira, A.S., González-Benito, M.E., Molina-García, A.D., 2014. Measurement of cooling and warming rates in vitrification-based plant cryopreservation protocols. Biotechnol. Prog. 30, 1177–1184. http://dx.doi.org/10.1002/btpr.1938.
Vernerey, F.J., Farsad, M., 2011. An Eulerian/XFEM formulation for the large deformation of cortical cell membrane. Comput. Methods Biomech. Biomed. Eng. 14, 433–445. https://doi.org/10.1080/10255842.2010.531273.

Vincze, G., Szasz, N., Szasz, A., 2005. On the thermal noise limit of cellular membranes. Bioelectromagnetics 26, 28–35. http://dx.doi.org/10.1002/bem.20051.

Wang, Y., Qin, Z., Buehler, M.J., Xu, Z., 2016. Intercalated water layers promote thermal dissipation at bio-nano interfaces. Nat. Commun. 7, 12854. https://doi.org/10.1038/ncomms12854.

Wei, R.X., Zhao, X.M., Hao, H.S., Du, W.H., Zhu, H.B., 2016. Embryonic stem-like cells from rabbit blastocysts cultured with melatonin could differentiate into three germ layers in vitro and in vivo. Mol. Reprod. Dev. 83, 1003–1014. http://dx.doi.org/10.1002/mrd.22739.

Xu, F., Moon, S., Zhang, X., Shao, L., Song, Y.S., Demirci, U., 2010. Multi-scale heat and mass transfer modelling of cell and tissue cryopreservation. Philos. Trans. R. Soc., A 368, 561–583. http://dx.doi.org/10.1098/rsta.2009.0248.

Xu, F., Sridharan, B., Wang, S., Gurkan, U.A., Syverud, B., Demirci, U., 2011. Embryonic stem cell bioprinting for uniform and controlled size embryoid body formation. Biomicrofluidics 5, 022207. http://dx.doi.org/10.1063/1.3580752.

Yamamoto, Y., Gotoh, S., Korogi, Y., Seki, M., Konishi, S., Ikeo, S., Sone, N., Nagasaki, T., Matsumoto, H., Muro, S., 2017. Long-term expansion of alveolar stem cells derived from human iPS cells in organoids. Nat. Methods 14, 1097–1106. http://dx.doi.org/10.1038/nmeth.4448.

Yang, Q.Z., Lian, Q., Xu, F., 2017. Perspective: fabrication of integrated organ-on-a-chip via bioprinting. Biomicrofluidics 11, 031301. http://dx.doi.org/10.1063/1.4982945.

Zhang, A., Cheng, S., He, L., Luo, D., Gao, D., 2004. Determination of thermal conductivity of cryoprotectant solutions and cell suspensions. Cell Preserv. Technol. 2, 157–162. http://dx.doi.org/10.1089/153834404774101990.

Zhang, W., Wang, S., Lin, M., Han, Y., Zhao, G., Jian Lu, T., Xu, F., 2012a. Advances in experimental approaches for investigating cell aggregate mechanics. Acta Mech. Solid. Sin. 25, 473–482. http://dx.doi.org/10.1016/S0894-9166(12)60042-1.

Zhang, X., Catalano, P.N., Gurkan, U.A., Khimji, I., Demirci, U., 2011. Emerging technologies in medical applications of minimum volume vitrification. Nanomedicine 6, 1115–1129. http://dx.doi.org/10.2217/nnm.11.71.

Zhang, X., Khimji, I., Shao, L., Safaee, H., Desai, K., Keles, H.O., Gurkan, U.A., Kayaalp, E., Nureddin, A., Anchan, R.M., 2012b. Nanoliter droplet vitrification for oocyte cryopreservation. Nanomedicine 7, 553–564. http://dx.doi.org/10.2217/nnm.11.145.

Zhou, X., Liu, Z., Liang, X.M., Shu, Z., Du, P., Gao, D., 2013. Theoretical investigations of a novel microfluidic cooling/warming system for cell vitrification cryopreservation. Int. J. Heat. Mass Transf. 65, 381–388. http://dx.doi.org/10.1016/j.ijheatmasstransfer.2013.06.022.